Xu, Luoyu R.; Islam, Md Shariful; Martinez, Ricardo; Flores, Mark; Zhao, Kai; Karakoc, Alp; Taciroglu, Ertugrul

Simplified indentation mechanics to connect nanoindentation and low-energy impact of structural composites and polymers

Published in:
JOURNAL OF REINFORCED PLASTICS AND COMPOSITES

DOI:
10.1177/07316844211072250

Published: 01/10/2022

Document Version
Peer reviewed version

Please cite the original version:
Xu, L. R., Islam, M. S., Martinez, R., Flores, M., Zhao, K., Karakoc, A., & Taciroglu, E. (2022). Simplified indentation mechanics to connect nanoindentation and low-energy impact of structural composites and polymers. *JOURNAL OF REINFORCED PLASTICS AND COMPOSITES*, *41*(19-20), 765-770. https://doi.org/10.1177/07316844211072250

Final version to Journal of Reinforced Plastics and Composites (JRP-21-0634)

Simplified Indentation Mechanics to Connect Nanoindentation and Low-energy Impact of Structural Composites and Polymers

*L. R. Xu[1] *, M. S. Islam[2], R. Martinez[3], M. Flores[4], K. Zhao[5] , A. Karakoç[6], E. Taciroglu[7]*

[1]School of Mechanical Engineering and Mechanics, Ningbo University, Ningbo, Zhejiang, 315000, CHINA

[2]Khulna University of Engineering & Technology, Khulna 9203, BANGLADESH.

[3]Department of Mechanical Engineering, University of Texas, El Paso, TX 79968, USA

[4] Air Force Research Laboratory, Wright-Patterson AFB, OH 45433, USA

[5]Structural Composites LLC, Houston, TX 77055, USA

[6]Department of Communications and Networking, Aalto University, 02150, FINLAND

[7]Department of Civil and Environmental Engineering, University of California, Los Angeles, CA 90095, USA

Graphical Abstract (2/25/2022)

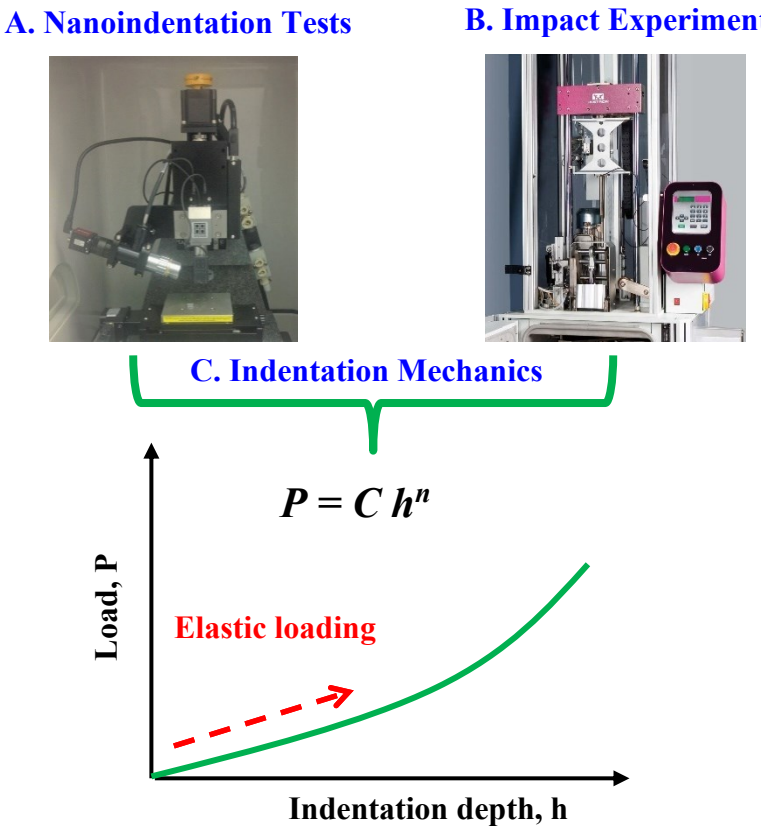

*corresponding author, electronic mail: l.roy.xu@alumni.caltech.edu

ABSTRACT

Nanoindentation (nanometer scale, extremely small) and impact (microsecond scale, extremely fast) experiments are two important techniques for characterizing modern material systems. However, these two experiments were often studied individually. In this pilot study, a multiscale indentation mechanics approach is proposed to correlate these two very different mechanics events acting on the same target materials using a spherical indenter and a projectile. The contact stiffness of nanoindentation of a target material is fitted using Hertz's contact law, and then the contact stiffness of impact is obtained using a simplified multiscale relation. Therefore, the maximum impact force of a projectile impact can be predicted by inputting the impact energy and the contact stiffness of impact. The above new approach was validated by drop-weight impact experiments of polymers and structural composite materials subjected to low-energy impact. Results show that only a few minutes are needed to predict the maximum impact force.

Keywords: Composite materials, Indentation mechanics, low-energy Impact, Nanoindentation.

1. INTRODUCTION

In recent years, composite materials, especially polymeric matrix composites, have been extensively used in aircraft, cars, ships, and wind turbine blades [1]. While these materials have many attractive features, they have a major shortcoming, that is, it has a low impact resistance along the thickness direction [2-15]. Therefore, the low-speed impact response of composite materials is a long-term research topic. In out-of-plane impact experiments of composite materials, a spherical impactor is used; therefore, researchers employed Hertz's contact law to characterize the low-speed impact response if no penetration occurred [16-18]. The low-speed impact event is also viewed as "dynamic indentation" [19]. As shown in Figure 1 and the included video, one of the authors conducted low-speed impact on a model composite specimen using dynamic

photoelasticity and ultra-high-speed photography. The video consists of a set of high-speed photos (https://www.youtube.com/watch?v=Fc5Uk1rMp_0). After a spherical impactor contacted the model matrix layer (the transparent polymer Homalite) of the specimen [20], the first event was stress wave propagation, and the second event was elastic dynamic indentation, which is the major research focus of this study. The third event was a complicated damage process, but it will be our future research as this paper only reports a pilot study. The black area in Figure 1 was the result of large out-of-plane deformation due to damage.

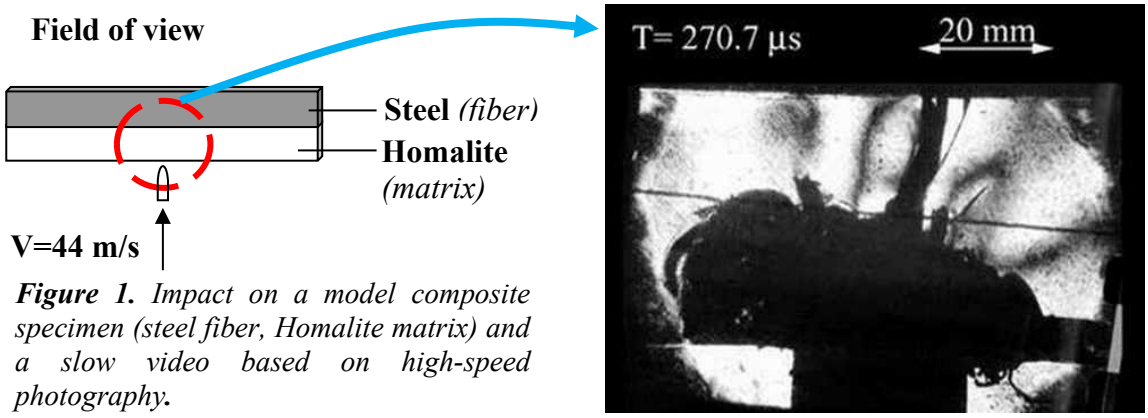

Figure 1. *Impact on a model composite specimen (steel fiber, Homalite matrix) and a slow video based on high-speed photography.*

On the other hand, nanoindentation is an efficient technique for measuring the mechanical properties of materials and devices at small length scales [21-31]. Indeed, the mechanics foundation of nanoindentation is still Hertz's contact law, which connects the indentation force and deformation. Previous research has shown that the classical Hertz's contact law is applicable to both small time-scale impact (microseconds) and small length-scale nanoindentation (nanometers), as reported by two major books on composite impact and nanoindentation [18, 32]. Therefore, we attempt to find the correlation between these two very different events using the multiscale indentation mechanics theory and conduct both impact and nanoindentation experiments for the same material systems to support our findings. First, we conducted

nanoindentation experiments on one polymer and two polymeric matrix composites. Second, we predicted the maximum impact force of the same material systems using multiscale indentation mechanics. Third, we performed low-speed impact experiments of the same material systems used in the nanoindentation experiments to validate the impact force prediction.

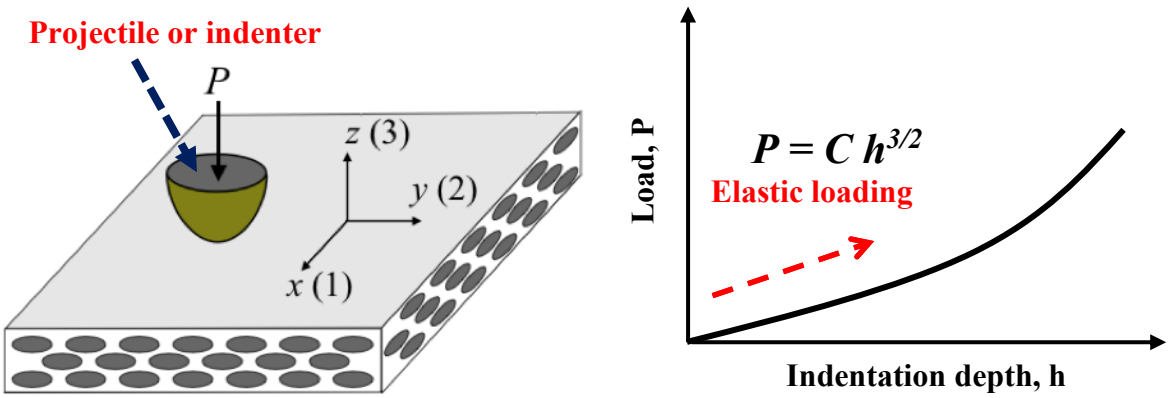

Figure 2. *Static (nanoindentation) and dynamic indentation (low-energy impact) along the Z (or 3) direction of a composite laminate (left), and a typical indentation force and depth curve (right).*

2. THEORETICAL BACKGROUND

2.1 Indentation mechanics for isotropic materials and orthotropic composite materials

As shown in Figure 2, the indentation load P of a spherical indenter is a function of the elastic indentation depth h and the indenter radius R based on Hertz's contact law [32]:

$$P = \frac{4}{3}\sqrt{R}\, E_r^{ID}\, h^{\frac{3}{2}} = C_{ID}\, h^{\frac{3}{2}}, \quad (1)$$

where C_{ID} is the contact stiffness of nanoindentation, the reduced modulus E_r is determined by the Young's modulus E and Poisson's ratio ν of the isotropic and homogenous target and indenter materials, and the subscript i refers to the indenter:

$$\frac{1}{E_r} = \frac{1-\nu_i^2}{E_i} + \frac{1-\nu^2}{E}. \quad (2)$$

For orthotropic fibrous composite laminates, as shown in Figure 2, a material coordinate system 1–2–3 is often employed. Here, 1 (or x) refers to the major fiber direction, 2 (or y) refers to the transverse in-plane direction, or the minor fiber direction (less fibers compared to those in the 1-

direction), and 3 (or z) refers to the thickness direction. Because the indenter is perpendicular to the composite laminate, the measured Young's modulus is the through-thickness Young's modulus E_3. Based on the classical work of Willis [33] and Yang and Sun [2], Hertz's contact law is applicable to static and dynamic indentation without penetration (low-energy impact) of orthotropic composite materials/laminates. Recently, Xu et al. [34] employed an approximate expression of the reduced modulus as a function of E_3 because no sophisticated models are available for the current composite indentation experiments:

$$\frac{1}{E_r} \approx \frac{1-v_i^2}{E_i} + \frac{1}{E_3}. \quad (3)$$

The approximate expression was validated by spherical nanoindentation experiments to measure the through-thickness Young's modulus of a glass fiber composite material (E-glass fiber/vinyl ester), and the measured modulus was consistent with the previously reported value of a similar material system. To measure the elastic constants, nanoindentation tests should be conducted within the elastic range, so the maximum indentation depth should be small, and the loading/unloading curves should be very close. Figure 3 shows a typical elastic nanoindentation loading/unloading curves of a CFRP composite specimen.

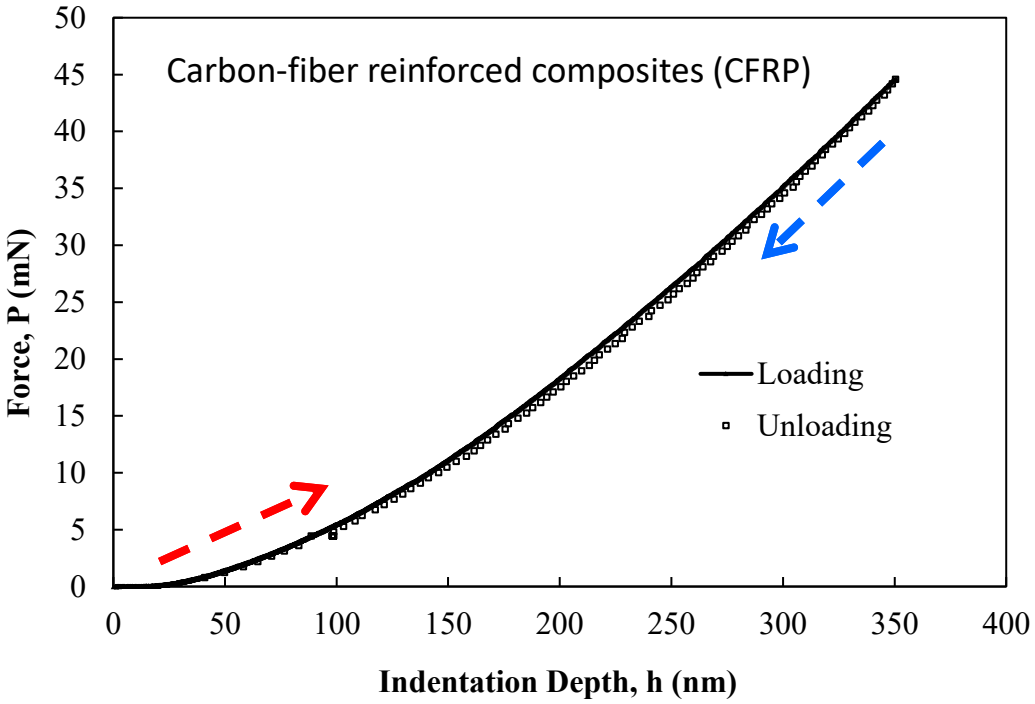

Figure 3. *Typical elastic nanoindentation loading/unloading curves of a CFRP composite*

2.2 Maximum impact force as a function of contact stiffness and impact energy

During a projectile impact process without penetration, the maximum impact load, P_{max}, is achieved at the zero relative speeds of the projectile and target. Andrews et al. [35] applied Newton's second law and contact mechanics principles on a moving sharp indenter. We employed the results of Abrate [18] on a moving spherical indenter and found that the maximum impact force was determined by the impact energy of the projectile W and the contact stiffness of impact C_{IP} between the projectile and the target:

$$P_{max} = \lambda \sqrt[5]{W^3 C_{IP}^2} \quad , \tag{4}$$

where λ is a constant (not a fitting parameter) that is independent of the boundary and support conditions (λ =1.73 for a spherical indenter or a spherical projectile), and C_{IP} is calculated based on Hertz's law:

$$C_{\mathrm{IP}} = \frac{4}{3}\sqrt{R_{\mathrm{IP}}}\, E_r^{IP}, \tag{5}$$

where R_{IP} refers to the radius of the projectile with a spherical head.

2.3 Multiscale indentation mechanics of two different techniques for the same material

Based on Equations (1) and (5), the contact stiffness of impact C_{IP} can be obtained from the contact stiffness of nanoindentation C_{ID} for the same target material system:

$$C_{IP} = C_{ID}\sqrt{R_{IP}/R_{ID}}\,[E_r^{IP}/E_r^{ID}], \tag{6}$$

where E_r^{ID} and E_r^{IP} are the reduced moduli of indentation and impact, respectively. Generally, the Young's moduli of common hard polymers such as poly(methyl methacrylate) (PMMA) and common composite matrices such as epoxy are less than 5 GPa. Moreover, the through-thickness moduli of common polymeric matrix composite systems are mainly controlled by their matrices [1], and thus their values are usually less than 20 GPa. In most nanoindentation experiments, the Young's modulus of a diamond nanoindenter is at least 1,000 GPa, while in a steel projectile impact test, the Young's modulus of steel is 200 GPa. Hence, we can obtain some simplified relations between two reduced moduli for the same target material, as expressed in Equation (6). Furthermore, the two contact stiffness values were found to have a simple relation: $C_{IP} \approx 0.95\, C_{ID}\sqrt{R_{IP}/R_{ID}}$ for glass and carbon fiber/vinyl ester composite laminates. For PMMA, $C_{IP} \approx 0.98\, C_{ID}\sqrt{R_{IP}/R_{ID}}$. Quinn et al. [36] conducted micro-indentation experiments at different loading rates for different materials, and found that there was a negligible effect on their Young's moduli. The two radii of the nanoindenter R_{ID} and the projectile R_{IP} form a multiscale relation. Therefore, a multiscale indentation mechanics approach is proposed to connect the two different mechanics experiments, which consists of

1) Obtaining the contact stiffness of nanoindentation C_{ID} by fitting Equation (1) and calculating the contact stiffness of impact C_{IP} using Equation (6).
2) Predicting the maximum impact force using Equation (4) by inputting the impact energy level and the contact stiffness of impact.
3) Validating the maximum impact force using drop-weight impact experiments.

EXPERIMENTAL STUDIES

3.1 Elastic nanoindentation experiments of polymer/polymeric matrix composites

We conducted spherical nanoindentation experiments on square specimens of 10 mm × 10 mm × 6.4 mm. The material systems were (1) PMMA, (2) two types of woven composite laminates for structural applications that were produced using vacuum-assisted resin transfer molding (VARTM) of (a) glass fiber reinforced vinyl ester (eight plies, fiber fraction $V_f = 0.54$), and (b) carbon fiber reinforced vinyl ester (same layout). As the first step, the contact stiffness of the target materials for nanoindentation was fitted using the measured nanoindentation load and displacement curves, as shown in Figure 3. It is important to note that Hertz's contact law is only applicable to the elastic loading stage. If the indentation load is high, the unloading curve will lead to permanent deformation when the indentation load is reduced to zero. Therefore, we limited our indentation depth h to approximately several hundred nanometers to avoid permanent deformation. Additional elastic nanoindentation details were reported by Martinez and Xu [37] and Xu et al. [34]. Here, we summarize the complicated composite indentation experiments. To reduce the inhomogeneous feature of the composite modulus measurement, we recommend using a spherical indenter with a large radius (200 μm in our experiments). Nanoindentation experiments were conducted with a separation between two indents of 200 μm along the x and y directions in the central area of each

specimen. The maximum indentation depth was approximately 150 nm, which was measured by the nanoindenter. Our previous finite element analysis showed that the above indentation deformation was purely elastic [37]. As the average diameter of a glass or carbon fiber is approximately 10 μm, the edge length of a square composite representative volume element (RVE) based on a fiber volume of 54% was approximately 12.5 μm. The radius of our spherical nanoindenter was 200 μm (R_{ID}), and thus our results did not lead to significant material inhomogeneity. In addition, at the maximum indentation depth of 150 nm, the diameter of the indenter/specimen contact area (close to a circle owing to the current woven fabric properties) was 16 μm (value calculated based on Fisher-Cripps [32]), which was sufficient to deform the RVE. Moreover, we indented at least 100 locations on each specimen, and at least three identical specimens were employed for each material system.

3.2 Low-energy impact experiments on a hard polymer and polymeric matrix composites

The impact event was introduced using an INSTRON drop-weight tester with a hemispherical steel projectile *(*R_{IP} of 7.95 mm and weight of 3.1 kg). The sizes of all rectangular impact specimens were 102 mm (width) × 152 mm (length) × 6.4 mm (thickness) according to ASTM standard 7136 for composite impact experiments [38]. The support and boundary conditions of the specimens were as follows: (1) four-edge clamped, or (2) four-edge free with back steel plates (see Figure 4). This impact fixture was fixed to a steel base inside the drop-weight tower. The impact energy levels of the steel projectile varied between 1, 2, 3, 4, and 5 J. Each impact occurred in the center of the specimen, and for each energy level, five identical specimens were employed. The impact force and energy as a function of time were recorded by the test machine. The impact experiments were conducted with low energy because (1) in this pilot study, ensuring elastic

deformation/no damage is critical for success, and (2) this energy level is related to accident drops of cell phones/tablets, while many protective cases are made of soft or hard polymers or fiber-reinforced composite materials.

4. RESULTS AND DISCUSSION

We only required some minutes to predict the maximum impact force using Equation (4). Figure 4 shows that our predictions were very close to the experimental data of PMMA plates, and the two types of boundary conditions yielded slightly different impact forces. The maximum impact force of the PMMA plate with free boundary conditions was always lower than that of the same PMMA plate with fixed boundary conditions because the first plate was easy to deform. Figure 5 shows a similar trend for the two types of composite laminates with the same clamped boundary conditions. It is not surprising that the two types of composite materials had a very similar impact force under the same impact energy level because their through-thickness Young's moduli were mainly controlled by their matrices (the same matrix in this study) according to the mechanics of composite materials [1]. Thus, the contact stiffness of impact of the two composite laminates was very close, and the maximum impact force values were almost the same according to Equation (4). Moreover, the contact stiffness of impact has a power of 2/5, and thus some difference in contact stiffness only leads to little change in the maximum impact force.

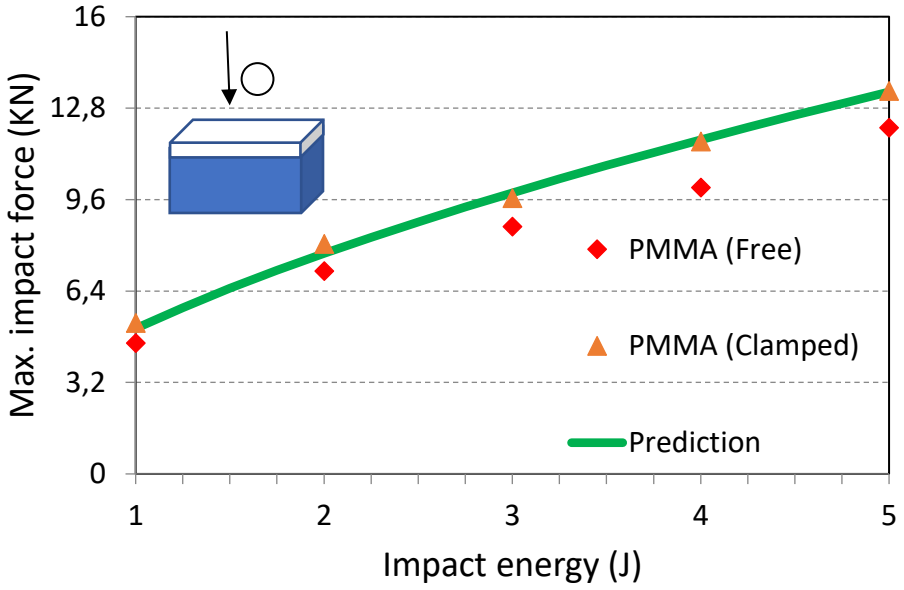

Figure 4. *Measured (points) and predicted (curve) maximum impact force as a function of impact energy for PMMA plates with two types of boundary conditions.*

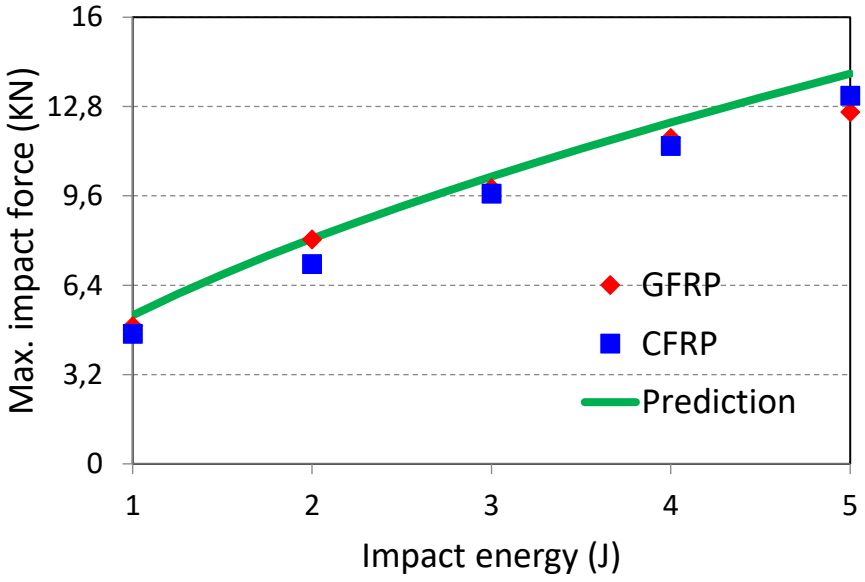

Figure 5. *Measured (points) and predicted (curve) maximum impact force as a function of impact energy for two types of composite material plates with four edges clamped.*

After visually examining the impacted specimen surface using the barely visible impact damage (BVID) concept, no damage was found in the three types of materials if the impact energy was less than 3 J. When the impact energy exceeded 3 J, small dents were observed. For the increased

impact energy (> 3 J), the predicted impact force was always higher than the measured one because the prediction was based on Hertz's elastic contact law. Further, plasticity or damage was introduced if the impact energy was high enough. In fact, plasticity or damage reduces the maximum impact force as it is an energy dissipation mechanism. For example, if the impact energy level is high, matrix cracks and delamination occur [18, 39, 40]. Therefore, for a high-energy impact case (e.g., > 5 J), our efficient impact force approach will provide a conservative upper-bound estimation to ensure structural or material safety because the measured impact force is always lower than the predicted force.

Indeed, the proposed efficient approach highlights the local dynamic indentation effect and ignores the global bending/shear deformation during the impact process [18, 35]. This equivalent force approach is similar to the common mechanics of material approach to calculate the maximum impact stress of a slender beam subjected to a rigid projectile impact (one-point impact at the beam center). When the speeds of the projectile and the target become zero, the kinetic energy of the projectile is fully converted to the strain energy of the beam (potential energy), and a statically equivalent maximum force is obtained for the beam impact case [41]. The maximum impact stress of the beam can be calculated easily using classical beam theory and the equivalent maximum force. However, the local dynamic indentation, which is based on elasticity theory, is ignored in the mechanics of the material approach. Actually, these two simplified approaches are opposite and applicable to two extreme cases.

We notice that the equivalent force approach has two requirements: (1) the target plate should be sufficiently thick so that the bending/shear deformation is small, and (2) the impact speed is not

high, or there is no penetration. For major aerospace composite applications, laminates are often very thick according to one co-author who works at the US Air Force Research Laboratory, and therefore their bending/shear deformation induced by a local projectile impact is small [38]. Moreover, the majority of studies on impact of aerospace composite laminates are low-energy impact cases; therefore, the proposed multiscale indentation mechanics principles will have suitable applications for different types of hard polymers and polymeric matrix composites.

5. CONCLUSIONS

A simplified multiscale indentation mechanics approach shows that spherical nanoindentation and low-energy impact using a spherical projectile are correlated by Hertz's contact law. The above approach was validated by nanoindentation and drop-weight impact experiments of a hard polymer and two types of polymeric matrix composites subjected to low-energy impact. Only a few minutes are needed to predict the maximum impact force. Moreover, the proposed efficient impact force approach will provide a conservative upper-bound estimation to ensure structural safety.

ACKNOWLEDGMENT

The authors acknowledge the constructive comments from two reviewers to improve the original manuscript.

Ethical Statement/Conflict of Interest

The authors do not have conflicts of interest

Data Availability Statement

The raw/processed data required to reproduce these findings cannot be shared at this time due to technical or time limitations.

REFERENCES

1. Daniel, I.M., Ishai, O., 2005. *Engineering Mechanics of Composite Materials*. Oxford University Press, New York.

2. Yang, S.H. and Sun, C.T., 1982. Indentation law for composite laminates. *ASTM STP*, *787*(1), pp.425-49.
3. Geubelle, P.H. and Baylor, J.S., 1998. Impact-induced delamination of composites: a 2D simulation. *Composites Part B: Engineering*, *29*(5), pp.589-602.
4. Li, G., Pang, S.S., Helms, J.E. and Ibekwe, S.I., 2000. Low velocity impact response of GFRP laminates subjected to cycling moistures. *Polymer composites*, *21*(5), pp.686-695.
5. Xu, L.R., Krishnan, A., Ning, H. and Vaidya, U., 2012. A seawater tank approach to evaluate the dynamic failure and durability of E-glass/vinyl ester marine composites. *Composites Part B: Engineering*, *43*(5), pp.2480-2486.
6. Guan, Z., He, W., Chen, J. and Liu, L., 2014. Permanent indentation and damage creation of laminates with different composite systems: An experimental investigation. *Polymer composites*, *35*(5), pp.872-883.
7. Zhang, J., Zhao, L., Li, M. and Chen, Y., 2015. Compressive fatigue behavior of low velocity impacted and quasi-static indented CFRP laminates. *Composite Structures*, *133*, pp.1009-1015.
8. Gu, G.X., Takaffoli, M., Hsieh, A.J. and Buehler, M.J., 2016. Biomimetic additive manufactured polymer composites for improved impact resistance. *Extreme Mechanics Letters*, *9*, pp.317-323.
9. Chen, Y., Hou, S., Fu, K., Han, X. and Ye, L., 2017. Low-velocity impact response of composite sandwich structures: modelling and experiment. *Composite Structures*, *168*, pp.322-334.
10. Miao, C. and Tippur, H.V., 2018. Measurement of sub-micron deformations and stresses at microsecond intervals in laterally impacted composite plates using digital gradient sensing. *Journal of Dynamic Behavior of Materials*, *4*(3), pp.336-358.
11. Thorsson, S.I., Waas, A.M. and Rassaian, M., 2018. Low-velocity impact predictions of composite laminates using a continuum shell based modeling approach part A: Impact study. *International Journal of Solids and Structures*, *155*, pp.185-200.
12. Kedir, N., Kirk, C.D., Guo, Z., Kerschen, N.E., Sun, T., Fezzaa, K. and Chen, W., 2019. Real-time visualization of impact damage in monolithic silicon carbide and fibrous silicon carbide ceramic composite. *International Journal of Impact Engineering*, *129*, pp.168-179.
13. Zhai, X., Gao, J., Liao, H., Kirk, C.D., Balogun, Y.A. and Chen, W.W., 2019. Mechanical behaviors of auxetic polyurethane foam at quasi-static, intermediate and high strain rates. *International Journal of Impact Engineering*, *129*, pp.112-118.
14. Lin, S., Thorsson, S.I. and Waas, A.M., 2020. Predicting the low velocity impact damage of a quasi-isotropic laminate using EST. *Composite structures*, *251*, p.112530.
15. Zhang, D., Zheng, X., Zhou, J. and Zhang, W., 2021. Bridging the low-velocity impact energy versus impact damage and residual compression strength for composite laminates. *Journal of Reinforced Plastics and Composites*, *40*(9-10), pp.378-390.
16. Sun, C.T. and Chattopadhyay, S., 1975. Dynamic response of anisotropic laminated plates under initial stress to impact of a mass. *Journal of Applied Mechanics*, 42(3), pp. 693-698.
17. Sankar, B.V., 1992. Scaling of low-velocity impact for symmetric composite laminates. *Journal of reinforced plastics and composites*, *11*(3), pp.296-309.
18. Abrate, S., 1998. *Impact on composite structures*. Cambridge university press, New York.
19. Xu, L.R. and Rosakis, A.J., 2002. Impact failure characteristics in sandwich structures: part I: basic failure mode selection. *International journal of solids and structures*, *39*(16), pp.4215-4235.

20. Xu, L.R. and Rosakis, A.J., 2005. Impact damage visualization of heterogeneous two-layer materials subjected to low-speed impact. *International Journal of Damage Mechanics*, *14*(3), pp.215-233.
21. Oliver, W.C. and Pharr, G.M., 1992. An improved technique for determining hardness and elastic modulus using load and displacement sensing indentation experiments. *Journal of materials research*, *7*(6), pp.1564-1583.
22. Chen, X. and Vlassak, J.J., 2001. Numerical study on the measurement of thin film mechanical properties by means of nanoindentation. *Journal of Materials Research*, *16*(10), pp.2974-2982.
23. Muliana, A., Haj-Ali, R.M., Steward, R. and Saxena, A., 2002. Artificial neural network and finite element modeling of nanoindentation tests. *Metallurgical and Materials Transactions A*, *33*(7), pp.1939-1947.
24. Gregory, J.R. and Spearing, S.M., 2005. Nanoindentation of neat and in situ polymers in polymer–matrix composites. *Composites science and technology*, *65*(3-4), pp.595-607.
25. Nakamura, T. and Gu, Y., 2007. Identification of elastic–plastic anisotropic parameters using instrumented indentation and inverse analysis. *Mechanics of materials*, *39*(4), pp.340-356.
26. Poon, B., Rittel, D. and Ravichandran, G., 2008. An analysis of nanoindentation in linearly elastic solids. *International Journal of Solids and Structures*, *45*(24), pp.6018-6033.
27. Heinrich, C., Waas, A.M. and Wineman, A.S., 2009. Determination of material properties using nanoindentation and multiple indenter tips. *International Journal of Solids and Structures*, *46*(2), pp.364-376.
28. Cao, G., Chen, X., Xu, Z.H. and Li, X., 2010. Measuring mechanical properties of micro- and nano-fibers embedded in an elastic substrate: theoretical framework and experiment. *Composites Part B: Engineering*, *41*(1), pp.33-41.
29. Gao, Y.F., Larson, B.C., Lee, J.H., Nicola, L., Tischler, J.Z. and Pharr, G.M., 2015. Lattice rotation patterns and strain gradient effects in face-centered-cubic single crystals under spherical indentation. *Journal of Applied Mechanics*, *82*(6), pp. 1007-1016.
30. de Vasconcelos, L.S., Xu, R., Li, J. and Zhao, K., 2016. Grid indentation analysis of mechanical properties of composite electrodes in Li-ion batteries. *Extreme Mechanics Letters*, *9*, pp.495-502.
31. Du, Y., Xu, T., Shaw, T.M., Liu, X.H., Bonilla, G., Li, H. and Lu, H., 2017. A novel tri-layer nanoindentation method to measure the mechanical properties of a porous brittle ultra-low-k dielectric thin film. *Extreme Mechanics Letters*, *13*, pp.100-107.
32. Fisher-Cripps, A.C., 2011. Nanoindentation. Springer, New York.
33. Willis, J.R., 1966. Hertzian contact of anisotropic bodies. *Journal of the Mechanics and Physics of Solids*, *14*(3), pp.163-176.
34. Xu, L.R., Martinez, R. and Zhao, K., 2019. Measurements of Through-Thickness Young's Moduli of Fibrous Composite Laminates Using Nanoindentation. *Journal of Engineering Materials and Technology*, *141*(3).
35. Andrews, E.W., Giannakopoulos, A.E., Plisson, E. and Suresh, S., 2002. Analysis of the impact of a sharp indenter. *International journal of solids and structures*, *39*(2), pp.281-295.
36. Quinn, G.D., Patel, P.J. and Lloyd, I., 2002. Effect of loading rate upon conventional ceramic microindentation hardness. *Journal of Research of the national Institute of Standards and Technology*, *107*(3), p.299.

37. Martinez, R. and Xu, L.R., 2014. Comparison of the Young's moduli of polymers measured from nanoindentation and bending experiments. *MRS Communications*, *4*(3), pp.89-93.
38. Flores, M., Mollenhauer, D., Runatunga, V., Beberniss, T., Rapking, D. and Pankow, M., 2017. High-speed 3D digital image correlation of low-velocity impacts on composite plates. *Composites Part B: Engineering*, *131*, pp.153-164.
39. Yan, H., Oskay, C., Krishnan, A. and Xu, L.R., 2010. Compression-after-impact response of woven fiber-reinforced composites. *Composites Science and technology*, *70*(14), pp.2128-2136.
40. Rhymer, J., Kim, H. and Roach, D., 2012. The damage resistance of quasi-isotropic carbon/epoxy composite tape laminates impacted by high velocity ice. *Composites Part A: Applied Science and Manufacturing*, *43*(7), pp.1134-1144.
41. Beer, F.P., Johnston, E.R., 2014. Mechanics of Materials. McGraw-Hill, New York.